A shallow earthquake swarm close to hydrocarbon activities: discriminating between natural and induced causes for the 2018–19 Surrey, UK earthquake sequence

Stephen P. Hicks[1], James Verdon[2], Brian Baptie[3], Richard Luckett[3], Zoë K. Mildon[4], Thomas Gernon[5]

1. Department of Earth Science and Engineering, Imperial College London, U.K.
2. School of Earth Sciences, University of Bristol, UK.
3. British Geological Survey, Edinburgh, UK.
4. School of Geography, Earth and Environmental Sciences, University of Plymouth, Plymouth, UK
5. School of Ocean and Earth Science, University of Southampton, U.K.

Abstract

Earthquakes induced by subsurface industrial activities are a globally emotive issue, with a growing catalogue of induced earthquake sequences. However, attempts at discriminating between natural and induced causes, particularly for anomalously shallow seismicity, can be challenging. An earthquake swarm during 2018–19 in south-east England with a maximum magnitude of M_L 3.2 received great public and media attention because of its proximity to operating oilfields. It is therefore vital and timely to provide a detailed characterisation of the earthquake sequence at present, and to decide based on current evidence, whether the earthquakes were likely natural or induced. We detected 129 earthquakes and computed detailed source parameters of these events. Most earthquakes occurred at a shallow depth of 2.3 km, >1 km deeper than the geological formations targeted by the oilfields, and laterally >3 km away from the drill-sites. We combine the east-west trending cluster of the seismicity with 2-D seismic reflection profiles to find the causative fault system for the earthquakes. A *b*-value close to unity and strike-slip faulting mechanisms are consistent with tectonic reactivation along a pre-existing fault. Overall, we find no indicators in the earthquake parameters that would strongly suggest an induced source. Nor do we find any clear trends between drilling activities and seismicity based on operational logs provided by the operators. Injected volumes are near-zero and monthly production amounts are many orders of magnitude smaller than other reported cases of extraction-induced seismicity. On balance, and based on the available evidence, we find it currently unlikely that nearby industrial activities induced the seismic swarm. Most likely, the Surrey earthquakes offer a uniquely detailed insight into shallow seismicity within sedimentary basins. Nevertheless, the way that activity reporting by operators themselves is regulated remains a controversial issue when discriminating between natural and induced seismicity for industrial methods that have not been expected to induce earthquakes.

Introduction

In recent years, seismicity induced and triggered by industry has become a topic of great scientific and public interest around the world. Seismic events near industrial facilities alarm local communities yet discriminating between anthropogenic and natural seismicity is not a trivial task (Grigoli *et al.*, 2017). Research has showed many forms of industrial activities can induce that seismicity. These include: conventional hydrocarbon production (Segall, 1989), stimulating geothermal reservoirs (Häring *et al.*, 2008), hydraulic fracturing (Clarke *et al.*, 2014), CO_2 storage (Kaven *et al.*, 2015), coal mining (Wilson *et al.*, 2015), and wastewater injection (Keranen *et al.*, 2014). Induced seismicity has been observed to occur both within crystalline basement (Verdon, 2014) and the shallower sedimentary formations being targeted by these operations (Eaton *et al.*, 2018). The poro-elastic response of shallow sedimentary rocks to changes in fluid pressure over large distances is poorly understood (Goebel and Brodsky, 2018).

Conversely, anomalous seismic swarms occurring at shallow depth can have natural causes (e.g. Bent *et al.*, 2017). Natural earthquakes close to industrial sites heighten public concern and can cause financial loss to operating companies if mis-attributed as induced; an example being the 2015 M_w 6.1 Emilia, Italy earthquake (Dahm *et al.*, 2015; Grigoli *et al.*, 2017). Overall, the mechanisms and occurrence statistics of very shallow earthquakes are poorly constrained.

Criteria to discriminate induced versus natural seismicity includes answering qualitative questions (Davis and Frohlich, 1993; Verdon *et al.*, 2019), and more quantitative analyses such as earthquake source studies, numerical modelling and statistical tests (Grigoli *et al.*, 2017).

The UK is one such area where induced earthquakes are a highly contentious issue. The background seismicity rate is low, with the regional state of stress dominated by northwest-southeast compression from the Mid-Atlantic Ridge and the Mediterranean (Baptie, 2010). Most earthquakes occur in the north and west of mainland Britain (Figure 1). Anthropogenic earthquakes in the UK account for ~20% of all earthquakes in the

instrumental catalogue (Wilson *et al.*, 2015). The greatest contributor has been coal mining (Kusznir *et al.*, 1980; Verdon *et al.*, 2018) in central-northern England, South Wales, and Scotland (Figure 1). The maximum observed magnitude from coal mining induced seismicity is M_L 3.1 (Redmayne, 1988; Bishop *et al.*, 1993; Wilson *et al.*, 2015). For geothermal induced seismicity, over 11,000 microseismic events were detected during the Hot Dry Rock project in southwest England between 1982 and 1987 (Pine and Batchelor, 2001). The largest event had a magnitude of M_L 2.0.

For hydrocarbon extraction, the largest induced event was the 2001 M_w 4.3 Ekofisk, North Sea earthquake with water injection causing shallow slip in the overburden at <3 km depth (Ottemöller *et al.*, 2005). In 2011, the first UK onshore hydraulic fracturing of shale took place near Blackpool in northern England. Injection triggered an M_L 2.3 earthquake, ~1.8 km from the Preese Hall-1 well, at 3.6 km depth (Clarke *et al.*, 2014). Hydraulic fracturing and induced microseismicity resumed nearby in 2018 at Preston New Road, drawing public attention once again to anthropogenic earthquakes (Clarke et al., 2019, in review). Most past induced earthquakes in the UK are small (M_L <3.1) and occur at shallow depth (<3 km). Therefore, accurately characterising earthquake sources and understanding the causes of such weak near-surface seismicity is challenging in areas with sparse seismic station coverage.

One such example is a sequence of small earthquakes that began on 1 April 2018, a few kilometres from the villages of Newdigate and Charlwood in Surrey, UK (Figure 1, Figure 2). The British Geological Survey (BGS) detected 32 small earthquakes between April 2018 and May 2019. Nearby people in large settlements, such as Crawley, Dorking, and Gatwick Airport, felt many of the earthquakes. Residents described shaking from the largest earthquake (M_L 3.2) corresponding to a maximum intensity of 5 (*Strong* shaking) on the European Macroseismic Scale (EMS); (Grünthal, 1998); (http://earthquakes.bgs.ac.uk/research/SurreyEarthquakes.html; last accessed May 2019). The sequence attracted much public interest for several reasons. First, south-east and southern England, which encompasses the Weald and Wessex basins, has a relatively low background earthquake activity rate in comparison to other parts of Britain

(Musson and Sargeant, 2007). Few similar sequences have been recorded in the past (Figure 1). Second, oilfield development and production activities at the active fields of Brockham and Horse Hill lie within 10 km distance of the earthquake sequence (Figure 2). Whilst no operators in the Weald have conducted, nor applied to do hydraulic fracturing, the UK's Traffic Light Scheme for hydraulic fracturing-induced seismicity has received extensive media attention. 31 events in the Newdigate swarm had magnitudes that exceed the current M_L = 0.5 "red light" threshold. However, the nearest permanent station of the BGS national seismic network lies on the southern coast of England, over 50 km away (Figure 1). This network sparsity made it difficult to initially constrain depth and faulting mechanisms, which can help to discriminate between natural and induced causes (Frohlich *et al.*, 2016). The strong macroseismic intensity observations supported early shallow depth estimates (initially fixed to 5.0 km), raising further suspicions over possible induced seismicity (Verdon *et al.*, 2019).

After the tenth recorded earthquake, we installed a network of five temporary broadband seismometer stations in the epicentral region (Figure 2). Given the large interest in these earthquakes, here we analyse available seismic data to make a coherent seismological analysis of the 2018–19 Surrey earthquake sequence up to mid-May 2019. We interpret these events in terms of the regional geological structure of the Weald Basin. We compare the spatial-temporal evolution of the seismicity with reported activities associated with oilfield development and production at the nearby Horse Hill and Brockham sites to understand its cause.

Regional geological, industrial, and seismological context

The epicentral area of the Newdigate sequence in the Weald Basin comprises uplifted sedimentary rocks spanning south-east England, the eastern English Channel and northern France (Figure 1). A wealth of 2-D seismic data from the UK Onshore Geophysical Library (UKOGL, 2019) allows for a robust characterisation of basin structure. The top Palaeozoic basement beneath the centre of the Weald lies at 2,500–3,000 km depth (Butler and Pullan, 1990). An interpreted regional seismic profile that runs ~20 km west of Newdigate shows sedimentary fill extending to depths of >3,000 m in the basin centre (UKOGL, 2019). Oil drilling in the Weald has targeted Jurassic rocks, including conventional reservoirs such as the Portland Sandstone, and lower-permeability formations such as the Kimmeridge Clay (Andrews, 2014). The Mesozoic basin sediments sit unconformably on Devonian-to-Lower Carboniferous Palaeozoic sedimentary rocks, which have been deformed, but not metamorphosed, by the Variscan orogeny (Butler and Pullan, 1990). Boreholes have rarely penetrated pre-Variscan units, and therefore are less well studied.

The key structural features of the Weald Basin were originally formed during the Variscan (Hansen *et al.*, 2002), generating east-west trending thrust faults. These were re-activated as extensional faults during the Permian as post-orogenic collapse, forming the basin. We find large extensional structures running through the Triassic and Jurassic sediments, rooted in the underlying basement and preserving the original east-west trend, with most dipping to the south.

Angus Energy plc. operates the Brockham oilfield, ~8 km away from the earthquakes (Figure 2). Brockham has produced relatively small volumes from the Portland Sandstone, with ~60,000 m^3 gross water and oil since 2002. Produced formation water produced is re-injected back into the reservoir. Overall, net output is greater than net injection. Production volumes since 2002 have been in decline, with several pauses in operations over the years. The most recent pause in operations occurred between February 2016 and March 2018. In 2017–2018, development work from a side-track well targeted the deeper Kimmeridge Clay Formation.

Known colloquially as the "Gatwick Gusher", the Horse Hill-1 (HH-1) development well lies ~3 km away from the earthquake swarm (Figure 2). Operated by UK Oil & Gas plc. (UKOG), HH-1 was first drilled in October 2014. UKOG first flow-tested the Portland Sandstone at ~600 m depth in March 2016 and the Kimmeridge Shale at ~800 m depth in July 2018. To date, ~7,000 m^3 of oil has been produced at HH-1 since July 2018. According to the operator, no water is currently being produced at the well, and no fluids are operationally injected into the reservoir.

Southern and south-east England is one of the least seismically active areas in the UK (Figure 1). The largest instrumentally recorded event in the region was the M_L 4.3 earthquake in Folkestone in 2009. The depth of this event was constrained by both teleseismic observations and regional waveform modelling at 5 ±2 km (Ottemöller *et al.*, 2009). There is also considerable evidence for damaging earthquakes in the Dover Straits over the last 1000 years, for example an estimated M_L 5.8 earthquake in 1580 (García-Moreno *et al.*, 2015). There are only a few recorded earthquakes within the Weald Basin itself. In 2005, there were three small earthquakes near Billingshurst (Figure 1, Label *a*), ~20 km west of the Newdigate sequence. The largest earthquake of the Billingshurst sequence had a magnitude of M_L 2.1 and a shallow depth – likely less than 5–10 km (Baptie and Luckett, 2018). Historical catalogues provide evidence for past earthquakes in the Weald region over the last 500 years. For example, Musson (Musson, 2008) finds reports of an earthquake on 5 May 1551. Although the limited macroseismic data means that a location and magnitude cannot be determined, the reports suggest that it was strongly felt with an intensity of 5 EMS in Dorking, ~8 km from the 2018–19 earthquake swarm. Further afield, there were six earthquakes near Chichester on the south coast (Figure 1, Label *b*) in the 1800s with estimated magnitudes of M_L 2.9–3.4 (Musson, 1994). Such earthquake sequences or swarms are relatively common in Great Britain. Examples include Comrie, 1788-1801 and 1839-46 (Musson, 1993); Kintail, 1974 (Assumpção, 1981) Manchester, 2002-2003 (Baptie and Ottemoeller, 2003) and Aberfoyle, 2003 (Ottemöller and Thomas, 2007). More recently, in 2014-2015 there was a sequence of earthquakes near Oakham in the East Midlands of England. The three largest events had magnitudes of 3.2, 3.5 and 3.8 ML, with depths of less than 5 km.

None of the above sequences were linked to anthropogenic causes, although the Manchester sequence occurred in a sedimentary basin where coal had been mined in the past.

Data and methods

Seismic waveform data for the first events comes mainly from the BGS national broadband seismic network (Figure 1). In south-east England, there are several RaspberryShake (RS) stations with geophone sensors (Anthony *et al.*, 2018), which improve the recording coverage of the earthquakes (Figure 1). The closest RS station (AM.REC60) lies ~6 km from the epicentral region of the swarm (Figure 2). After the first nine events, we installed a network of five temporary stations in the area (Figure 2) comprising Güralp 3ESPC 30 s – 100 Hz seismometers, with a sampling rate of 200 Hz. We installed two of these stations (GB.HORS and GB.RUSH) in mid-July and three (GB.GATW, GB.STAN, GB.BRDL) in early August 2018 (Figure 3a). We analysed seismic waveform data up until 13/05/2019 (see Data and Resources).

We derive our 1-D seismic velocity model from detailed sonic log information from nearby boreholes (Note S1, Figure S1 & Table S1 in the electronic supplement to this article). To relocate the earthquakes, we used NonLinLoc (Lomax *et al.*, 2009), which offers robust constraints on location uncertainties compared with traditional single-event location codes. To assess any smaller-scale structure in the spatial-temporal evolution of the seismicity, we also computed double-difference relocations (Waldhauser and Ellsworth, 2000); (Note S1 in the electronic supplement to this article). ~19,000 delay time pairs each for P- and S-waves and ~15,000 and ~18,000 cross-correlation times for P- and S-waves, respectively, were selected for the double-difference relocation. We computed magnitudes using the UK local magnitude (M_L) scale of Luckett et al. (2019), suitable for near-field observations (Note S2 in the electronic supplement to this article).

To detect further low-magnitude seismicity not in the initial BGS catalogue, we took two approaches. (1) We used the Lassie software (Heimann, 2016), a stack-and-delay-based coherence detector, to find and locate events using continuous data from the temporary seismic network. Coherency is mapped using a smooth characteristic function calculated from normalised waveform envelopes. From this catalogue, we then (2) ran a cross-correlation template-matching algorithm on data from local stations. For this, we used 1.0 s-long template waveforms incorporating P- and S-waves from the events in the

catalogue. We utilised EQcorrscan (Chamberlain *et al.*, 2018) to scan for earthquakes on data filtered at 5–15 Hz. Detections were made when the network-stacked cross-correlation sum exceeds nine times the median absolute deviation. We then manually re-picked and relocated positive detections. For nearby RS station AM.REC60, we also scanned continuous waveforms before the first known earthquake, extending back as far as September 2017, when this station was first installed. There were no earlier positive detections; therefore, no significantly large earthquake (M_L>1.5) likely occurred here before 01/04/2018, so the main sequence started then.

To investigate the causal mechanism of the Newdigate earthquakes, we computed moment tensors from waveforms, Gutenberg-Richter *b*-values, stress drops from displacement spectra, and static stress transfer (see Notes S3, S4 & S5 in the electronic supplement to this article).

Results

Besides the 34 events recorded in the BGS catalogue, we detected a further 95 micro-earthquakes from 12/07/2018 onwards, forming an overall catalogue of 129 events (Figure 2, Figure 3b; Table S2 in the electronic supplement to this article). Hypocentres for well-constrained events recorded by five temporary monitoring stations have a mean depth of 2.3 km. Most locations have formal epicentral and depth uncertainties of <200 m and <500 m, respectively. These solutions are robust as they vary little when relocated in different velocity models, and they had low root-mean-square arrival time residuals (<60 ms). Given the high waveform similarity between large events (Figure 4), we fixed the depth of events before 12/08/2018 to 2.3 km (Note S1 in the electronic supplement to this article).

Overall, the best-constrained events illuminate a seismogenic patch ~2.5 km long and extending over 1.3 km in depth (Figure 2). Most event epicentres in our full catalogue appear to cluster along a roughly linear band, trending east-west. A few microseismic events were detected up to 2 km away to the north and east of the main cluster of seismicity. High-precision double-difference relocations of 95 events confirm the strong east-west alignment of seismicity (Figure S2 in the electronic supplement to this article).

The temporary stations captured six of the larger earthquakes (M_L ≥1.9) in July 2018 and February 2019 (Figure 3a-b), allowing us to probe rupture mechanisms and depths (see Figure 5 for examples). The best-constrained moment tensor solutions have centroid depths of 2.2±0.2 km, consistent with hypocentre depths (Figure S7 in the electronic supplement to this article) and show the same strike-slip faulting mechanism. The west-east nodal plane corresponds to the alignment of seismicity (Figure 2). The double-couple percentage is high (>75%). Analysis of 218 P-wave polarities from the wider catalogue suggest that most events had this same mechanism, with little variability (Figure 5c).

In Figure 2, we examine whether this cluster of earthquakes correlates with pre-existing faults identified from 2-D seismic profiles (Note S6 in the electronic supplement to this article). Faults within the Mesozoic sediments are relatively easy to find, most of which strike east-west and dip towards the south. We also find north-dipping and ENE–WSW

trending faults. The Newdigate Fault (NGF) is a prominent east-west striking, south-dipping fault system showing a normal sense of offset, which extends across much of the study area. Most epicentres lie along the projected surface trace of the NGF, consistent with the west-east nodal plane of the focal mechanisms, suggesting slip occurred along this fault system (Figure 2, Figure 5). We can see this overall relationship more clearly in the double-difference relocations (Figure S2 in the electronic supplement to this article).

The Triassic lowermost basin fill and underlying Palaeozoic rocks appear to be more heavily faulted (Figure 6). Given the spacing of the 2-D seismic lines and the number of fault traces, we have not attempted to map every fault in the lower units. However, we can assume that these faults have similar trends and positions as the extensional faults that extend above them. The double-difference locations show that most events occurred within the footwall of the NGF; they likely occurred on a south-dipping fault at greater depth within the lowermost basin fill (Figure 6).

From fitting displacement spectra of earthquakes in the sequence (see Figure S3 in the electronic supplement to this article for an example), we compute stress drops of 0.2–11.0 Mpa (Figure S6 in the electronic supplement to this article). From modelled static stress changes resulting from the M_L >2 earthquakes, accounting for the depth and the fault geometry uncertainties, we find that most events with M_L >2 occurred in a region of positive static stress from earlier earthquakes (Figure S8 in the electronic supplement to this article). For M_L >2 earthquakes, we computed the total accumulated static stress at the hypocentre before each earthquake (Table S3 in the electronic supplement to this article) resolved onto fault geometries consistent with the Newdigate and Horse Hill faults. For nearly all M_L >2 earthquakes, changing the depth and/or strike of the receiver faults within the range of uncertainties can cause positive stress changes. For some earthquakes, the epicentres were too close, and therefore the static stress calculated is unreliable (Steacy *et al.*, 2004).

We also assess the frequency-magnitude distribution of the Newdigate seismic sequence in terms of the *b*-value of the Gutenberg-Richter relationship. We look at several timeframes for this as the temporary local monitoring network was not in place for the

start of the earthquake sequence. We compute magnitude of completeness, M_c by minimising the residual between a power law fit to the data and the observed distribution (Wiemer and Wyss, 2000). First, we consider the entire earthquake sequence starting in April 2018. We find an M_c of ~2.2, supported by the overall M_c estimate for south-east England (Survey, 2010). Here, we find a best-fitting *b*-value of 1.1 (Figure 7a).

For the time when the local temporary monitoring network was operational, we computed a much lower M_c of -0.2. This is supported by the detection of few M_L <0.2 events outside of the hours of 1300 – 0500 (Figure S4 in the electronic supplement to this article) because of higher daytime cultural noise. Previous studies (Staudenmaier *et al.*, 2018) show that the different scaling between M_L and M_W for small earthquakes may cause an artificial bi-linear Gutenberg-Richter fit. Therefore, we also used our spectral and moment tensor estimates of M_w to re-scale the M_L values. For this part of the catalogue, we are still cannot include the larger magnitudes with a single Gutenberg-Richter fit. We assume that this effect is due to M_c varying with time and our relatively small catalogue of earthquakes under-sampling the true earthquake sequence with an exponential distribution. In any case, we truncate the maximum magnitude at M_L 1.1. This yields a *b*-value of 0.9 (Figure 7b).

Discussion

Based on the location of our interpreted subsurface faults and earthquake locations, we identify the NGF zone as the causative structure for most of the earthquakes. Given this correlation, and computed moment tensors, the earthquakes most likely represent right-lateral strike-slip faulting along this west-east striking structure. In cross-section, the double-difference relocations imply a steeply dipping fault plane (Figure 6, and Figure S2 in the electronic supplement to this article). At the earthquake source depths, according to interpreted well logs from HH-1 and Brockham, the rock types are mainly mudstone-rich Middle-Lower Jurassic to Upper Triassic sedimentary rocks. The stronger limestone unit of the Penarth Formation at ~2.3 km depth could promote the more brittle failure required for seismic slip.

There are few cases of very shallow (<3 km depth) earthquake sequences documented in the literature, likely a result of sub-optimal station coverage needed to accurately resolve such shallow depths. Many documented cases of shallow seismicity in stable continental regions worldwide link such seismicity with induced causes, such as hydraulic fracturing (Clarke *et al.*, 2014; Eaton *et al.*, 2018), conventional oil production (Frohlich *et al.*, 2012), hydraulic fracturing (Clarke *et al.*, 2014; Eaton *et al.*, 2018), and groundwater extraction (González *et al.*, 2012). There are fewer documented cases of anomalously shallow natural earthquakes within sedimentary basins, with most past cases confined to metamorphic (Maceira *et al.*, 2000; Bent *et al.*, 2017) and igneous lithologies (Malone *et al.*, 1975). Most earthquakes in the UK are consistent with rupture in the shallow to mid-crust, although many events have shallower, and often poorly constrained depths. Earthquakes occurring at such depths are thought to be relatively rare in the UK, with the most accurate depths for background seismicity lying between 5 and 15 km. However, re-analysis of the 2005 Billingshurst sequence, 20 km to the west of Newdigate, has suggested shallow event depths (Baptie and Luckett, 2018).

Given the location of the earthquakes, it is important to assess whether nearby oilfield activities induced these events or whether they were natural. We first consider the problem within the framework of the criteria established by Frohlich et al. (2016) since

these were designed for both injection- and extraction-based operations, without requiring knowledge of well pressures.

1. Past precedence. There are no known past earthquakes associated with oil and gas activities in south-east England, also an area of low seismicity (Figure 1). The 2005 Billingshurst earthquakes in the Weald are the nearest analogue to the Newdigate events as they occurred at a shallow depth but not close to any known hydrocarbon activities. The long-term magnitude of completeness of the British Geological Survey seismicity catalogue for the entire UK is likely M_L ~3.0 (Musson and Sargeant, 2007); therefore, we cannot rule out smaller past earthquakes in the area. Induced seismicity has been associated with hydraulic fracturing for shale gas in northern England (Clarke *et al.*, 2014) and conventional hydrocarbon extraction in the North Sea (Ottemöller *et al.*, 2005; Wilson *et al.*, 2015). Yet no documented cases exist of conventional onshore extraction inducing seismicity on the British Isles. Compared to offshore plays, onshore reservoirs in the UK typically produce hydrocarbons at much smaller volumes and rates.
2. Spatial correlation with industrial activities**.** Figure 1 shows that the Newdigate earthquake cluster occurred 3–5 km away from HH-1 and 6-8 km from the Brockham site. We find no events at closer distances to HH-1; nor do we find any systematic migration of seismicity with time either away from or towards HH-1. The earthquakes are 1.0–1.5 km deeper than the Portland and Kimmeridge targets, which lie at 550–700 m and 700–1000 m depth, respectively (Figure 6). The earthquakes also likely occurred within either Triassic sedimentary rocks or the underlying deformed Palaeozoic rocks. Again, the linear group of epicentres appear to line up along the mapped NGF (Figure 2).
3. Temporal links with industrial activities. Whilst oil licence sites lie close to the seismic cluster, we also need to consider whether the earthquakes temporally correlate with oilfield activities. Figure 3 shows a timeline of seismicity and nearby well operations. After a two-year pause, production and associated injection activities resumed at the Brockham site in March 2018, two weeks before the first earthquake on 01/04/2018. Therefore, a coincidence exists between the start of

the seismicity and the restart in activities at Brockham. However, fluids have been produced at Brockham for 14 years previously without inducing known seismicity. Nevertheless, induced seismicity has been shown to often lag by many years the start of production in conventional, large hydrocarbon reservoirs (Maury *et al.*, 1990). Work was carried out at HH-1 in March 2018 (Figure 3), shortly before the first earthquake on 1 April. According to operator logs, this work involved only preparing the site at the surface and no subsurface work in the borehole took place. Flow testing at HH-1 in February–March 2016 and in July 2018 was a long time both before and after the start of the earthquakes (Figure 3), so we find no direct temporal correlation. Looking at events with magnitudes much greater than M_c, we find that 30–50% of earthquakes in our catalogue occurred within 72 hours of a reported well shut-in day at HH-1, whereas only 13–30% of events occurred during a period of oil production (Figure 3). However, robustly determining any such correlation is uncertain. It depends on the lower magnitude threshold chosen, and it is difficult to remove the effect of aftershocks occurring very soon after mainshocks. For hydraulic fracturing and wastewater injection, seismicity rates generally diminish during well shut-in periods (Horton, 2012; Schultz *et al.*, 2016). For simultaneous extraction and injection, models show that the highest pore pressure disturbance along basement faults may occur after shut-in (Chang and Segall, 2016). For gas extraction, well shut-ins lead to an overall decrease in earthquakes, although some critically stressed faults may rupture many years later (Zbinden *et al.*, 2017).

Using the Frohlich et al. (2016) criteria, uncertainty arises from the testing the questions posed, as we could classify the Newdigate sequence as either “Possibly Induced” or “Probably Induced”. However, this approach is likely an over-simplification as it does not consider detailed source parameters or knowledge of fluid pressure or pathways (Verdon *et al.*, 2019). We therefore assess the seismic source parameters in whether they show an induced or natural cause for the events. We then examine in more detail whether the oilfield activities conducted at HH-1 and Brockham had the potential to induce earthquakes.

The faulting mechanisms (Figure 2, Figure 5) are similar to the overall pattern in the British Isles, in which strike-slip faulting dominates (Fig. 1); (Baptie, 2010). The Newdigate earthquake focal mechanisms are consistent with the regional stress field with the maximum horizontal stress oriented northwest-southeast. None of our moment tensor solutions show a large non-double-couple component (Figure 5), as is sometimes observed for induced earthquakes (Sileny, 2009; Wang *et al.*, 2018). In cases where seismicity is induced by compaction in a conventional reservoir, we expect normal faulting at the edges of the reservoir, and reverse faulting within the overburden (Segall, 1989). Such mechanisms have been observed for compaction-induced events at large, depleting hydrocarbon fields (Ottemöller *et al.*, 2005; Wees *et al.*, 2014; Dahm *et al.*, 2015; Willacy *et al.*, 2018). However, for the Newdigate events, the lack of such dip-slip components in the computed focal mechanisms shows that a compaction/subsidence mechanism did not cause the earthquakes. A faulting mechanism consistent with the regional state of stress does not completely dictate a natural cause. Induced earthquakes because of fluid injection or hydraulic fracturing also usually have a rupture geometry and sense-of-slip consistent with regional stress directions (Clarke *et al.*, 2014; McNamara *et al.*, 2015). However, there has been no large fluid injection at HH-1. Injection at Brockham is of produced water, with the volume injected being smaller than the volume produced from the same formation (Figure 3), resulting in net fluid withdrawal.

The mean stress drop of 3.2 MPa, given the uncertainty in corner frequency estimates, is consistent with a wide range values computed for past earthquakes in Britain (Baptie *et al.*, 2005; Ottemöller *et al.*, 2009). We can attribute the relatively low stress drop to the low shear strength of sedimentary rocks (Ottemöller *et al.*, 2005). Debate continues on whether we can use stress drop as an indicator of the events being induced. Hough (2014) suggests that induced earthquakes may have stress drops up to ten times weaker than natural events of similar magnitudes based on ground shaking intensity. However, Zhang et al. (2016) found no significant stress drop variation between induced and natural earthquakes. Regardless, we find no evidence for an abnormal stress drop for the Newdigate events.

The Gutenberg-Richter *b*-value can give insights into the underlying causes of earthquakes. Seismicity caused by tectonic stresses on pre-existing faults usually has a *b*-value close to unity. Conversely, seismicity induced by fluid-related processes, whether natural (Wyss *et al.*, 1997) or because of fluid injection (Maxwell *et al.*, 2012), often has a higher *b*-value. The high magnitude of completeness and relatively small size of our catalogue means that our computed *b*-value is poorly constrained, but our best estimates suggest it is close to the global average of 1.0. However, this does not on its own rule out a causal link with industrial activities, as many cases of induced seismicity produce *b*-values close to 1. But overall this b-value suggests seismicity controlled by tectonic stresses along a pre-existing fault, consistent with the imaged fault structures (Figure 2, Figure 6).

In summary therefore, our observations of seismic source parameters are consistent with natural tectonic earthquakes. Given the regional stress tensor, uncertainties in the style of faulting and the static stress changes associated with the M>2 earthquakes in this sequence, it is likely that static stress triggering played a role (Figure S8 in the electronic supplement to this article). We are not required to invoke fluid pressure changes, which have explained the spatial-temporal evolution of injection-induced seismicity (Catalli *et al.*, 2013).

To our knowledge, seismicity caused by extraction has only been reported at very large hydrocarbon fields where production has taken place for many years. In contrast, the relatively small extraction volumes and rates at Brockham and HH-1 (Figure 3) likely do not promote overburden failure. Compared to large oilfields globally, the Brockham reservoir is small, with only ~60,000 m^3 reported oil and water produced, with low rates of extraction, since 2002 (Figure 3). This volume is several orders of magnitude smaller than reservoirs where well-documented production-induced seismicity has occurred (Segall, 1989). At Brockham, production over roughly 15 years has been balanced by re-injection of produced formation water back into the reservoir. Also, the injection of produced water into a depleted reservoir from which oil has been extracted is unlikely to increase the pressure in the reservoir to above pre-production levels, making induced

seismicity less likely (Rubinstein and Mahani, 2015). Overall, more fluid has been extracted than withdrawn, so the net fluid balance is negative, and pore pressures in the Brockham field are likely lower than when the reservoir was first produced from. As a result, injection at Brockham can be ruled out as a cause. Many E-W and ENE–WSW striking faults between Brockham and the Newdigate Fault (Figure 6) likely act as a baffle to fluids or hydraulic pressure migrating towards the earthquake source region.

At HH-1, during the 2016 flow test, the operator injected approximately 150 m^3 acid and water to open fractures in the Kimmeridge at a rate of 0.24 m^3/min and pressure of 10 MPa. A short-period of flow then followed this testing. Compared to well-studied cases of injection-induced seismicity in the U.S. (Frohlich, 2012), these volumes and rates at HH-1 are much smaller. Also, the flow testing that followed the acid injection would likely offset any transient pressure increase. With a gap of over two years between fracture acidisation at HH-1 and the first earthquake, a mechanism involving a time lag of such duration is unlikely given the small volumes injected.

The earthquakes began in April 2018, pre-dating phase two of flow testing at HH-1 on 09/07/2018 (Figure 3). The second major cluster of earthquakes had also occurred by this time. Based on available operational data, this eliminates HH-1 as a direct cause for these events.

The toe of the HH-1 well is close to the Horse Hill Fault but does not intersect it (Figure 2), although we cannot estimate a fault damage zone width. Hypothetically, a structural connection between the Horse Hill and Newdigate Faults could support this triggering mechanism by acting as a conduit for fluid and pressure changes. Based on the available 2-D seismic profiles, although we cannot completely rule out a diffuse fault transfer zone between the north-dipping Horse Hill fault and south-dipping NGF, we find no clear evidence to suggest that these faults intersect at depth.

The final possibility is that the first events of the seismic sequence were natural, but then flow testing work at HH-1 subsequently induced a resumption of seismicity. If so, the only causative mechanism would be one of extraction and pore pressure drawdown (Teufel *et al.*, 1991). Induced seismicity at conventional hydrocarbon fields is typically produced by

compaction and slip within the overburden, which requires high production volumes from large, laterally extensive fields. At HH-1, the volumes produced to date are small (~7,000 m^3), and oil has only been produced for a very short time. We are not aware of any extraction-and-subsidence related seismicity for such small fluid volumes reported in the scientific literature. As discussed above, we would expect to have dip-slip motions associated with compaction, rather than the observed strike-slip mechanisms. In such cases, we expect seismicity to occur within and above the zone affected by pore pressure drawdown. For such volumes, this zone is unlikely to extend more than a few hundred metres from the well-bore; not 3 km away laterally and over 1 km below the reservoir.

Conclusions

Based on the available evidence and consideration of possible triggering mechanisms, we conclude that at present, it is unlikely that anthropogenic activities induced the 2018–2019 Newdigate seismic sequence. We draw this conclusion from the following key observations of seismicity and hydrocarbon operations:

1. *Timing of the start of seismic activity*. Based on operators' logs, the earthquake sequence started before subsurface activity and flow testing/production at HH-1 in 2018.
2. *Location*. The earthquakes occur at least 3 km from the nearest oilfield operations, which would be an abnormally long distance for production-induced seismicity based on past reported cases. The earthquakes did not occur directly above, within, or on the immediate flanks of the extraction reservoir, which could show an induced cause (Segall and Fitzgerald, 1998). We see no migration in the seismicity with time towards or away the oil reservoirs.
3. *Temporal correlation with ongoing oilfield activities*. Based on detailed operational logs provided by the operators, we find no clear link between seismicity rate and cumulative oil production or activities at either HH-1 or Brockham. Some earthquakes occurred during well shut-in periods at HH-1, however if this is a factor, the stress transfer mechanism is unclear.
4. *Source mechanisms*. Highly double-couple strike-slip focal mechanisms are consistent with the regional state of stress and background seismicity in the UK. We do not find dip-slip faulting mechanisms that are observed for cases of production-induced seismicity (Segall, 1989). The frequency-magnitude character of the seismicity is not abnormal and shows a tectonic control on the earthquakes, consistent with reactivation of a pre-existing fault. The presence of multiple faults imaged using 2-D seismic and double-difference relocations can help to explain the swarm-like nature of the seismic sequence.
5. *Fluid volumes and stress*. The reported cumulative volumes of net production are many orders of magnitude smaller than past reported cases of extraction-induced

seismicity. Therefore, for such volumes, we do not expect large-scale poro-elastic stress changes >10 MPa, which might be needed to induce seismicity (Segall, 1989). Aside from a small volume injected for fracture acidisation at HH-1 in 2016, long before the first earthquake, and small volumes of fluid re-injection at Brockham that are exceeded by production volumes, the volumes and rates involved are very small. These amounts are dwarfed by other reported cases of fluid injection-induced seismicity over large distances (Goebel and Brodsky, 2018). Static stress modelling shows that earthquakes likely triggered each other by loading multiple fault strands rather than any external driver of fluid pore pressure changes.

6. *Fluid pathways.* There is no obvious connection between the Horse Hill and Newdigate Faults which could plausibly offer a permeability pathway from HH-1 to the earthquakes. Many west-east trending normal faults likely act as a baffle to fluid flow to/from Brockham.

If all or some earthquakes were induced or triggered, then it would represent a novel mechanism not previously recognised for this style of oil extraction at the reported volumes. We have shown that seismic activity can occur at shallow depths in sedimentary basins, especially where pre-existing faults are optimally oriented for reactivation in the regional stress field. This result has implications for understanding the background rate of seismicity close to hydrocarbon exploration targets. Such shallow seismicity could pose a moderate seismic hazard to areas of high population density. Moreover, operators and regulators could consider operating small seismic monitoring networks near conventional oilfield operations to better understand any nearby emergent seismic sequences earlier and to reduce uncertainties.

The 2018–19 Newdigate seismic sequence was a contentious issue among members of the public, oilfield operators, and campaign groups. Without detailed seismic observations offered by the installed temporary seismic network and nearby citizen seismology sensors, large uncertainty over the causes of the sequence may have remained for the foreseeable future. Our knowledge of activities at Brockham and HH-1 relies on reported

operational data provided by the operators. This source of data remains a controversial issue when determining induced versus natural causes of earthquakes. This particularly applies to industrial activities that lack any precedence for causing earthquakes, and for areas with a low rate of background seismicity. As operations continue in the long term, we recommend seismic monitoring close to hydrocarbon development and production sites, and high-resolution reporting of operational activities (e.g. well shut-in periods), production volumes and rates. Over time, longer-term monitoring could help reduce uncertainties in correlations and casual factors. We have shown that the 2018–2019 Newdigate, Surrey earthquakes offer new insight into the seismogenic potential of shallow sedimentary basins and the seismic hazard associated with these swarms.

Data and resources

All seismic waveform data used in this study is available from the British Geological Survey (ftp://seiswav.bgs.ac.uk; last accessed May 2019) and from the RaspberryShake FDSN web service. All instrumentation for the temporary seismic stations was provided by the British Geological Survey. Operational data from Brockham and Horse Hill was provided by the operators of those fields, Angus Energy and UK Oil and Gas, respectively. We made figures using the Matplotlib (Hunter, 2007), GMT (Wessel and Smalley, 1998), and EQcorrscan (Chamberlain *et al.*, 2018) packages.

Electronic supplement

For this pre-print version, the electronic supplement can be accessed from the following link:

https://www.dropbox.com/sh/b7s1f6f5ajkzw6m/AABMdGcMfwSQeiL4WTuhyXIHa?dl=0

Acknowledgments

We thank UK Oil and Gas Plc. and Angus Energy Plc. for providing well data and sonic well logs. We are also grateful to the UK Oil and Gas Authority for organising a workshop on the Newdigate earthquakes, which resulted in very fruitful scientific discussions with all participants. We also thank Branden Christensen and Angel Rodriguez, and their team at RaspberryShake / OSOP, S.A. for their co-operation when working with the community data. We are grateful for discussions with Al Fraser on subsurface fault mapping, and with Antony Butcher on b-value determination. Finally, we thank Mr. Nicholas Booth, the owner of RS station AM.REC60 for continuing to maintain the monitoring effort throughout the Newdigate earthquake sequence. Thank you to David Hawthorn and his team at the BGS for installing the temporary seismic stations.

The Authors declare that there are no conflicts of interest.

References

Andrews, I. (2014). The Jurassic shales of the Weald Basin: geology and shale oil and shale gas resource estimation.

Anthony, R. E., A. T. Ringler, D. C. Wilson, and E. Wolin (2018). Do Low-Cost Seismographs Perform Well Enough for Your Network? An Overview of Laboratory Tests and Field Observations of the OSOP Raspberry Shake 4D, *Seismol Res Lett* **90**, no. 1, 219 228, doi: 10.1785/0220180251 .

Assumpção, M. (1981). The NW Scotland earthquake swarm of 1974, *Geophys J Int* **67**, no. 3, 577 586, doi: 10.1111/j.1365-246x.1981.tb06938.x .

Baptie, B. (2010). Seismogenesis and state of stress in the UK, *Tectonophysics* **482**, no. 1–4, 150 159.

Baptie, B., and R. Luckett (2018). The Newdigate earthquake sequence, 2018, British Geological Survey Internal Rept.

Baptie, B., and L. Ottemoeller (2003). The Manchester earthquake swarm of October 2002, *EGS-AGU-EUG Joint Assembly*.

Baptie, B., L. Ottemöller, S. Sargeant, G. Ford, and A. O'Mongain (2005). The Dudley earthquake of 2002: A moderate sized earthquake in the UK, *Tectonophysics* **401**, no. 1–2, 1 22.

Bent, A. L., S. Halchuk, V. Peci, K. E. Butler, K. B. Burke, J. Adams, N. Dahal, and S. Hayek (2017). The McAdam, New Brunswick, Earthquake Swarms of 2012 and 2015–2016: Extremely Shallow, Natural Events, *Seismol Res Lett* **88**, no. 6, 1586 1600, doi: 10.1785/0220170071 .

Bishop, I., P. Styles, and M. Allen (1993). Mining-induced seismicity in the Nottinghamshire Coalfield, *Q J Eng Geol Hydroge* **26**, no. 4, 253–279, doi: 10.1144/gsl.qjegh.1993.026.004.03 .

Butler, M., and C. P. Pullan (1990). Tertiary structures and hydrocarbon entrapment in the Weald Basin of southern England, *Geological Soc Lond Special Publ* **55**, no. 1, 371 391, doi: 10.1144/gsl.sp.1990.055.01.19 .

Catalli, F., M. Meier, and S. Wiemer (2013). The role of Coulomb stress changes for injection-induced seismicity: The Basel enhanced geothermal system, *Geophys Res Lett* **40**, no. 1, 72 77, doi: 10.1029/2012gl054147 .

Chamberlain, C. J., C. J. Hopp, C. M. Boese, E. Smith, D. Chambers, S. X. Chu, K. Michailos, and J. Townend (2018). EQcorrscan: Repeating and Near-Repeating Earthquake Detection and Analysis in Python, *Seismol Res Lett* **89**, no. 1, 173 181, doi: 10.1785/0220170151 .

Chang, K., and P. Segall (2016). Seismicity on Basement Faults Induced by Simultaneous Fluid Injection–Extraction, *Pure Appl Geophys* **173**, no. 8, 2621 2636, doi: 10.1007/s00024-016-1319-7 .

Clarke, H., L. Eisner, P. Styles, and P. Turner (2014). Felt seismicity associated with shale gas hydraulic fracturing: The first documented example in Europe, *Geophys Res Lett* **41**, no. 23, 8308 8314, doi: 10.1002/2014gl062047 .

Dahm, T., S. Cesca, S. Hainzl, T. Braun, and F. Krüger (2015). Discrimination between induced, triggered, and natural earthquakes close to hydrocarbon reservoirs: A probabilistic approach based on the modeling of depletion-induced stress changes and seismological source parameters, *J Geophys Res Solid Earth* **120**, no. 4, 2491 2509, doi: 10.1002/2014jb011778 .

Davis, S. D., and C. Frohlich (1993). Did (Or Will) Fluid Injection Cause Earthquakes? - Criteria for a Rational Assessment, *Seismological Research Letters* **64**, no. 3–4, 207 224.

Eaton, D. W., N. Igonin, A. Poulin, R. Weir, H. Zhang, S. Pellegrino, and G. Rodriguez (2018). Induced Seismicity Characterization during Hydraulic-Fracture Monitoring with a Shallow-Wellbore Geophone Array and Broadband Sensors, *Seismol Res Lett* **89**, no. 5, 1641 1651, doi: 10.1785/0220180055 .

Frohlich, C. (2012). Two-year survey comparing earthquake activity and injection-well locations in the Barnett Shale, Texas, *Proc National Acad Sci* **109**, no. 35, 13934 13938, doi: 10.1073/pnas.1207728109 .

Frohlich, C., H. DeShon, B. Stump, C. Hayward, M. Hornbach, and J. I. Walter (2016). A Historical Review of Induced Earthquakes in Texas, *Seismol Res Lett* **87**, no. 4, 1022 1038, doi: 10.1785/0220160016 .

Frohlich, C., J. Glidewell, and M. Brunt (2012). Location and Felt Reports for the 25 April 2010 mbLg 3.9 Earthquake near Alice, Texas: Was it Induced by Petroleum Production?The April 2010 Earthquake near Alice, Texas: Was it Induced by Petroleum Production?, *B Seismol Soc Am* **102**, no. 2, 457 466, doi: 10.1785/0120110179 .

García-Moreno, D., K. Verbeeck, T. Camelbeeck, Batist, F. Oggioni, Z. O. Hurtado, W. Versteeg, H. Jomard, J. Collier, S. Gupta, *et al.* (2015). Fault activity in the epicentral area of the 1580 Dover Strait (Pas-de-Calais) earthquake (northwestern Europe), *Geophys J Int* **201**, no. 2, 528–542, doi: 10.1093/gji/ggv041 .

Goebel, T. H., and E. E. Brodsky (2018). The spatial footprint of injection wells in a global compilation of induced earthquake sequences, *Science* **361**, no. 6405, 899 904, doi: 10.1126/science.aat5449 .

González, P. J., K. F. Tiampo, M. Palano, F. Cannavó, and J. Fernández (2012). The 2011 Lorca earthquake slip distribution controlled by groundwater crustal unloading, *Nat Geosci* **5**, no. 11, 821 825, doi: 10.1038/ngeo1610 .

Grigoli, F., S. Cesca, E. Priolo, A. Rinaldi, J. F. Clinton, T. A. Stabile, B. Dost, M. Fernandez, S. Wiemer, and T. Dahm (2017). Current challenges in monitoring, discrimination, and management of induced seismicity related to underground industrial activities: A European perspective, *Reviews of Geophysics* **55**, no. 2, 310 340.

Grünthal, G. (1998). European macroseismic scale 1998.

Hansen, D. L., D. J. Blundell, and S. B. Nielsen (2002). A model for the evolution of the Weald Basin, *Bulletin of the Geological Society of Denmark*.

Häring, M. O., U. Schanz, F. Ladner, and B. C. Dyer (2008). Characterisation of the Basel 1 enhanced geothermal system, *Geothermics* **37**, no. 5, 469 495, doi: 10.1016/j.geothermics.2008.06.002 .

Heimann, S. (2016). Sebastian Heimann / lassie.

Horton, S. (2012). Disposal of Hydrofracking Waste Fluid by Injection into Subsurface Aquifers Triggers Earthquake Swarm in Central Arkansas with Potential for Damaging Earthquake, *Seismol Res Lett* **83**, no. 2, 250 260, doi: 10.1785/gssrl.83.2.250 .

Hough, S. (2014). Shaking from Injection-Induced Earthquakes in the Central and Eastern United States, *B Seismol Soc Am* **104**, no. 5, 2619 2626, doi: 10.1785/0120140099 .

Hunter, J. D. (2007). Matplotlib: A 2D graphics environment, *Computing in science & engineering* **9**, no. 3, 90.

Kaven, J., S. Hickman, A. McGarr, and W. Ellsworth (2015). Surface Monitoring of Microseismicity at the Decatur, Illinois, CO 2Sequestration Demonstration Site, *Seismol Res Lett* **86**, no. 4, 1096 1101, doi: 10.1785/0220150062 .

Keranen, K., M. Weingarten, G. Abers, Bekins, and S. Ge (2014). Sharp increase in central Oklahoma seismicity since 2008 induced by massive wastewater injection, *Science* **345**, no. 6195, 448 451, doi: 10.1126/science.1255802 .

Kusznir, N., D. Ashwin, and A. Bradley (1980). Mining induced seismicity in the North Staffordshire coalfield, England, *International Journal of Rock Mechanics and Mining Sciences & Geomechanics Abstracts* **17**, no. 1, 45 55.

Lomax, A., A. Michelini, and A. Curtis (2009). Earthquake location, Direct, Global-search Methods, *Encyclopedia of complexity and systems science*, 2449 2473, doi: 10.1007/978-0-387-30440-3_150 .

Luckett, R., L. Ottemöller, A. Butcher, and B. Baptie (2019). Extending local magnitude ML to short distances, *Geophys J Int* **216**, no. 2, 1145 1156, doi: 10.1093/gji/ggy484 .

Maceira, M., C. J. Ammon, and R. Herrmann (2000). Faulting Parameters of the September 25, 1998 Pymatuning, Pennsylvania Earthquake, *Seismol Res Lett* **71**, no. 6, 742 752, doi: 10.1785/gssrl.71.6.742 .

Malone, S., G. Rothe, and S. W. Smith (1975). Details of microearthquake swarms in the Columbia Basin, Washington, *Am J Sci* **259**, no. 8, doi: 10.2475/ajs.259.8.583 .

Maury, V., J. Grasso, and G. Wittlinger (1990). Lacq Gas Field (France): Monitoring of Induced Subsidence and Seismicity Consequences on Gas Production and Field Operation, doi: 10.2118/20887-ms .

Maxwell, S., M. Jones, R. Parker, S. Miong, S. Leaney, D. Dorval, D. D'Amico, J. Logel, E. Anderson, and K. Hammermaster (2012). Fault activation during hydraulic fracturing,

SEG Technical Program Expanded Abstracts 2009 **43**, 1552 1556, doi: 10.1190/1.3255145 .

McNamara, D., H. Benz, R. Herrmann, E. Bergman, P. Earle, A. Holland, R. Baldwin, and A. Gassner (2015). Earthquake hypocenters and focal mechanisms in central Oklahoma reveal a complex system of reactivated subsurface strike-slip faulting, *Geophys Res Lett* **42**, no. 8, 2742–2749, doi: 10.1002/2014gl062730 .

Musson, R. (1994). A catalogue of British earthquakes, *British Geological Survey Global Seismology Report*.

Musson, R. M. W. (1993). Comrie: a historical scottish earthquake swarm and its place in the history of seismology, *Terra Nova* **5**, no. 5, 477–480, doi: 10.1111/j.1365-3121.1993.tb00288.x .

Musson, R. (2008). The seismicity of the British Isles to 1600, *British Geological Survey Open Report*.

Musson, R., and S. Sargeant (2007). Eurocode 8 seismic hazard zoning maps for the UK.

Ottemöller, L., B. Baptie, and N. Smith (2009). Source Parameters for the 28 April 2007 Mw 4.0 Earthquake in Folkestone, United Kingdom, *B Seismol Soc Am* **99**, no. 3, 1853 1867, doi: 10.1785/0120080244 .

Ottemöller, L., H. Nielsen, K. Atakan, J. Braunmiller, and J. Havskov (2005). The 7 May 2001 induced seismic event in the Ekofisk oil field, North Sea, *J Geophys Res Solid Earth 1978 2012* **110**, no. B10, 379, doi: 10.1029/2004jb003374 .

Ottemöller, L., and C. Thomas (2007). Highland Boundary Fault Zone: Tectonic implications of the Aberfoyle earthquake sequence of 2003, *Tectonophysics* **430**, no. 1–4, 83 95.

Pine, R., and A. Batchelor (2001). Downward migration of shearing in jointed rock during hydraulic injections, *International Journal of Rock Mechanics and Mining Sciences & Geomechanics Abstracts* **21**, no. 5, 249–263.

Redmayne, D. (1988). Mining induced seismicity in UK coalfields identified on the BGS National Seismograph Network, *Geological Soc Lond Eng Geology Special Publ* **5**, no.

1, 405–413, doi: 10.1144/gsl.eng.1988.005.01.45 .

Rubinstein, J. L., and A. Mahani (2015). Myths and Facts on Wastewater Injection, Hydraulic Fracturing, Enhanced Oil Recovery, and Induced Seismicity, *Seismol Res Lett* **86**, no. 4, 1060–1067, doi: 10.1785/0220150067 .

Schultz, R., R. Wang, Y. Gu, H. K. of Geophysical, and 2017 (2016). A seismological overview of the induced earthquakes in the Duvernay play near Fox Creek, Alberta, *Wiley Online Library*.

Segall, P. (1989). Earthquakes triggered by fluid extraction, *Geology* **17**, no. 10, 942, doi: 10.1130/0091-7613(1989)017<0942:etbfe>2.3.co;2 .

Segall, P., and S. D. Fitzgerald (1998). A note on induced stress changes in hydrocarbon and geothermal reservoirs, *Tectonophysics* **289**, no. 1–3, 117 128, doi: 10.1016/s0040-1951(97)00311-9 .

Sileny, J. (2009). Resolution of Non-Double-Couple Mechanisms: Simulation of Hypocenter Mislocation and Velocity Structure Mismodeling, *B Seismol Soc Am* **99**, no. 4, 2265 2272, doi: 10.1785/0120080335 .

Staudenmaier, N., T. Tormann, B. Edwards, N. Deichmann, and S. Wiemer (2018). Bilinearity in the Gutenberg-Richter Relation Based on ML for Magnitudes Above and Below 2, From Systematic Magnitude Assessments in Parkfield (California), *Geophys Res Lett* **45**, no. 14, 6887 6897, doi: 10.1029/2018gl078316 .

Steacy, S., D. Marsan, S. S. Nalbant, and J. McCloskey (2004). Sensitivity of static stress calculations to the earthquake slip distribution, *J Geophys Res Solid Earth 1978 2012* **109**, no. B4, 20,153, doi: 10.1029/2002jb002365 .

Survey, B. (2010). Detection Capability, *httpwww.earthquakes.bgs.ac.ukmonitoringdetectioncapability.html*.

Teufel, L. W., D. W. Rhett, and H. E. Farrell (1991). Effect of reservoir depletion and pore pressure drawdown on in situ stress and deformation in the Ekofisk field, North Sea, *The 32nd US Symposium on Rock Mechanics (USRMS)*.

UKOGL (2019). UK Onshore Geophysical Library.

Verdon, J. P. (2014). Significance for secure CO2 storage of earthquakes induced by fluid injection, *Environ Res Lett* **9**, no. 6, 064022, doi: 10.1088/1748-9326/9/6/064022 .

Verdon, J. P., B. J. Baptie, and J. J. Bommer (2019). An Improved Framework for Discriminating Seismicity Induced by Industrial Activities from Natural Earthquakes, *Seismol Res Lett*, doi: 10.1785/0220190030 .

Verdon, J. P., J.-M. Kendall, A. Butcher, R. Luckett, and B. J. Baptie (2018). Seismicity induced by longwall coal mining at the Thoresby Colliery, Nottinghamshire, U.K., *Geophys J Int* **212**, no. 2, 942 954, doi: 10.1093/gji/ggx465 .

Waldhauser, F., and W. L. Ellsworth (2000). A Double-Difference Earthquake Location Algorithm: Method and Application to the Northern Hayward Fault, California, *B Seismol Soc Am* **90**, no. 6, 1353 1368, doi: 10.1785/0120000006 .

Wang, R., Y. Gu, R. Schultz, and Y. Chen (2018). Faults and Non-Double-Couple Components for Induced Earthquakes, *Geophys Res Lett* **45**, no. 17, 8966 8975, doi: 10.1029/2018gl079027 .

Wees, V. J., L. Buijze, K. van Thienen-Visser, M. Nepveu, B. Wassing, B. Orlic, and P. Fokker (2014). Geomechanics response and induced seismicity during gas field depletion in the Netherlands, *Geothermics* **52**, 206 219, doi: 10.1016/j.geothermics.2014.05.004 .

Wessel, P., and R. Smalley (1998). New, improved version of generic mapping tools released, *Eos Trans. AGU* **79**, no. 47, 579 579.

Wiemer, S., and M. Wyss (2000). Minimum Magnitude of Completeness in Earthquake Catalogs: Examples from Alaska, the Western United States, and Japan, *B Seismol Soc Am* **90**, no. 4, 859–869, doi: 10.1785/0119990114 .

Willacy, C., E. van Dedem, S. Minisini, J. Li, J. Blokland, I. Das, and A. Droujinine (2018). Application of full-waveform event location and moment-tensor inversion for Groningen induced seismicity, *Lead Edge* **37**, no. 2, 92 99, doi: 10.1190/tle37020092.1 .

Wilson, M. P., R. J. Davies, G. R. Foulger, B. R. Julian, P. Styles, J. G. Gluyas, and S. Almond (2015). Anthropogenic earthquakes in the UK: A national baseline prior to shale exploitation, *Mar Petrol Geol* **68**, no. Bull. Earthq. Res. Inst. Tokyo Univ. 43 1965, 1 17, doi: 10.1016/j.marpetgeo.2015.08.023 .

Wyss, M., K. Shimazaki, and S. Wiemer (1997). Mapping active magma chambers by b values beneath the off-Ito volcano, Japan, *J Geophys Res Solid Earth* **102**, no. B9, 20413 20422, doi: 10.1029/97jb01074 .

Zbinden, D., A. Rinaldi, L. Urpi, and S. Wiemer (2017). On the physics-based processes behind production-induced seismicity in natural gas fields, *J Geophys Res Solid Earth* **122**, no. 5, 3792 3812, doi: 10.1002/2017jb014003 .

Zhang, H., D. W. Eaton, G. Li, Y. Liu, and R. M. Harrington (2016). Discriminating induced seismicity from natural earthquakes using moment tensors and source spectra, *J Geophys Res Solid Earth* **121**, no. 2, 972 993, doi: 10.1002/2015jb012603 .

Figure captions

Figure 1: Regional context showing the study area (brown rectangle), together with instrumental and historical seismicity context of England and Wales from the BGS catalogue. Induced earthquakes are from Wilson et al. (Wilson *et al.*, 2015) Regional seismic stations used in this study are shown. Mapped surface fault traces come from BGS (2019). Past earthquake focal mechanisms (orange beachballs) come from Baptie, 2010 and from BGS annual earthquake bulletin reports. Labels a) and b) refer to the 2005 Billingshurst and 1811–1834 Chichester sequence, respectively, which are discussed in the text.

Figure 2: Left: map of the study area showing relocated earthquakes of the 2018–2019 Newdigate sequence, focal mechanisms, mapped faults, local seismic stations, 2-D seismic lines (Note S6 in the electronic supplement to this article), and the locations of oilfield activities. Only high-quality earthquake hypocentres are plotted with a maximum azimuthal gap of less than 200°. Earthquake locations are coloured to show their evolution through time. Dark grey circles indicate earthquakes that occurred before the installation of the temporary local seismic network, and therefore have uncertain locations, with fixed depths. 2-D seismic profile TWLD-90-15 is shown in Figure 6. Right: N-S and W-E cross-sections of seismicity with event hypocentres. The cross-section locations are labelled on the map. The definition of fault abbreviations are as follows: BHF = Box Hill Fault; BRF = Brockham Fault; BUF = Buckland Fault; COF = Collendean Fault; FGF = Faygate Fault; HWF = Holmwood Fault; HHF = Horse Hill Fault; KFF = Kingsfold Fault; LHF = Leigh Fault; NGF = Newdigate Fault; OKF = Ockley Fault; WCF = Westcott Fault; WB1F = Whiteberry-1 Fault.

Figure 3: Timeline comparing evolution of the Newdigate seismic swarm with nearby oil field activities. a) Installation dates of the local temporary seismic monitoring network. (a) detected seismicity, cumulative number of events, and the grey shaded area indicating the approximate completeness magnitude of the catalogue over time. (c) Horse Hill-1: operations timeline (shaded boxes; see Table S4 in the Electronic Supplement to this article) together with flow-period averaged production and cumulative production over

time. d) Daily reservoir production and injection values at Brockham. (e) A long-term view of operations, with the time interval shown in panels above covering the 2018–2019 period delineated by the grey box and connecting lines.

Figure 4: Lowpass-filtered (10 Hz) vertical-component waveforms recorded at RaspberryShake (RS) station REC60 (~8 km epicentral distance) showing similarity between the largest events (M_L > 1.5) of the Newdigate sequence. Waveform cross-correlation (CC) values computed in a window starting 0.02 s and ending 0.70 s after the picked P-wave arrival are labelled and are calculated with respect to the first event in the sequence (#1).

Figure 5: a) and b) Representative moment tensor solutions for two earthquakes recorded by all five local stations. i) Map showing stations and best-fitting focal mechanism; ii) waveform correlation as a function of centroid depth; iii) waveform fits. “VR” = variance reduction. c) Observed first-motion P-wave polarities from all events in the catalogue represent a composite faulting mechanism compared to fault planes from the best-fitting focal mechanisms from moment tensors a) and b).

Figure 6: 2-D seismic section along profile TWLD-90-15 (Figure 2) showing interpreted faults (green lines), geological formations, together with the projected positions of double-difference relocated earthquakes from this study. The colour of each event denotes the time that each event occurred. COF = C = Collendean Fault; FGF = Faygate Fault; LHF = Leigh Fault; NGF = Newdigate Fault. An uninterpeted version of this section is shown in Figure S13.

Figure 7: Individual and cumulative frequency-magnitude distributions together with Gutenberg-Richter (G-R) relationship fits for a) the entire sequence and b) the sequence recorded by the temporary local monitoring network, with magnitudes scaled to an equivalent M_w, and G-R fits truncated to maximum magnitude of 1.2.

Figures

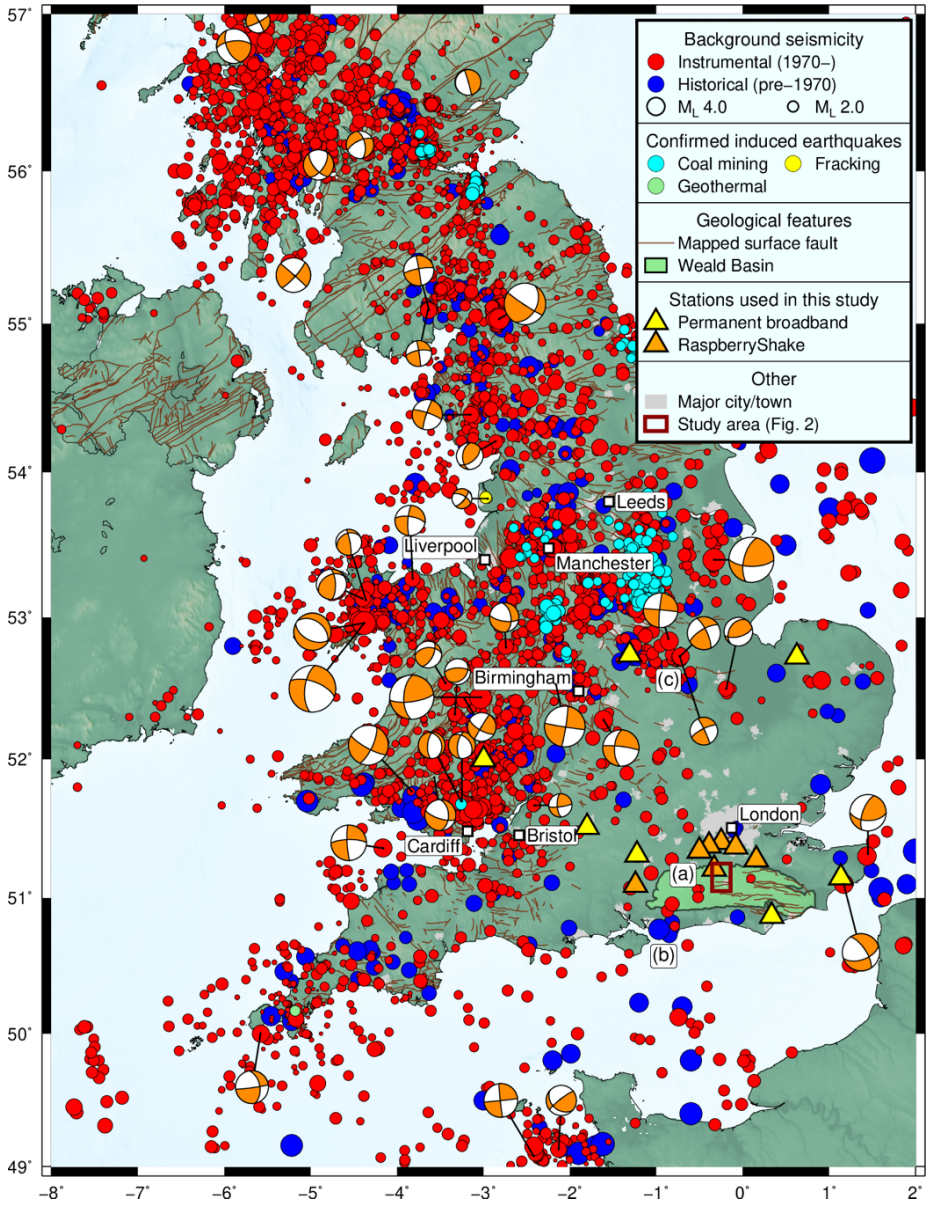

Figure 1: Regional context showing the study area (brown rectangle), together with instrumental and historical seismicity context of England and Wales from the BGS catalogue. Induced earthquakes are from Wilson et al. (Wilson *et al.*, 2015) Regional seismic stations used in this study are shown. Mapped surface fault traces come from BGS (https://www.bgs.ac.uk/data/services/kml/BGS_GEOLOGY_625_faults.kmz; last accessed May 2019). Past earthquake focal mechanisms (orange beachballs) come from Baptie, 2010 and from BGS annual earthquake bulletin reports. Labels a) and b) refer to the 2005 Billingshurst and 1811–1834 Chichester sequence, respectively, which are discussed in the text.

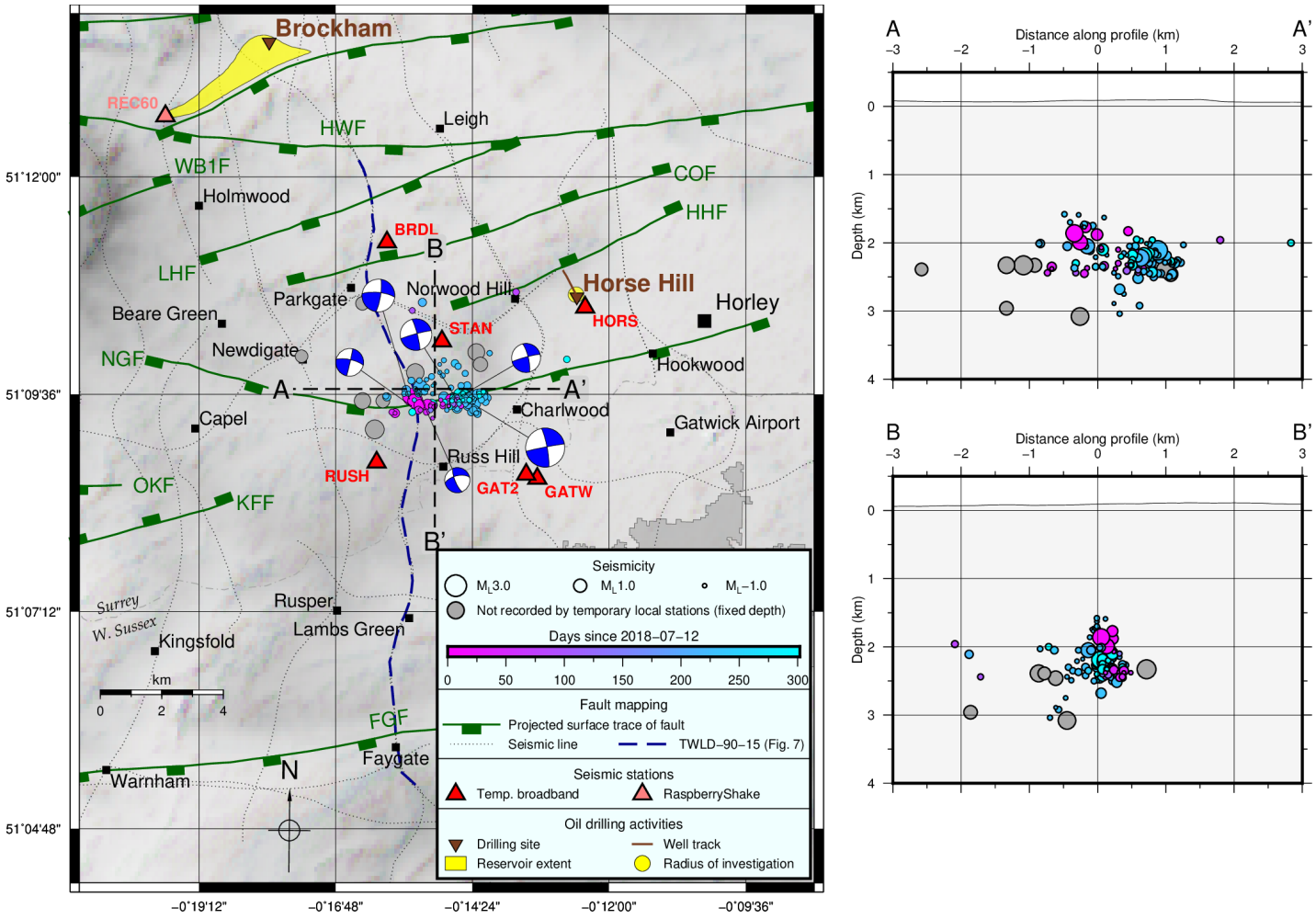

Figure 2: Left: map of the study area showing relocated earthquakes of the 2018–2019 Newdigate sequence, focal mechanisms, mapped faults, local seismic stations, 2-D seismic lines (Note S6 in the electronic supplement to this article), and the locations of oilfield activities. Only high-quality earthquake hypocentres are plotted with a maximum azimuthal gap of less than 200°. Earthquake locations are coloured to show their evolution through time. Dark grey circles indicate earthquakes that occurred before the installation of the temporary local seismic network, and therefore have uncertain locations, with fixed depths. 2-D seismic profile TWLD-90-15 is shown in Figure 6. Right: N-S and W-E cross-sections of seismicity with event hypocentres. The cross-section locations are labelled on the map. The definition of fault abbreviations are as follows: BHF = Box Hill Fault; BRF = Brockham Fault; BUF = Buckland Fault; COF = Collendean Fault; FGF = Faygate Fault; HWF = Holmwood Fault; HHF = Horse Hill Fault; KFF = Kingsfold Fault; LHF = Leigh Fault; NGF = Newdigate Fault; OKF = Ockley Fault; WCF = Westcott Fault; WB1F = Whiteberry-1 Fault.

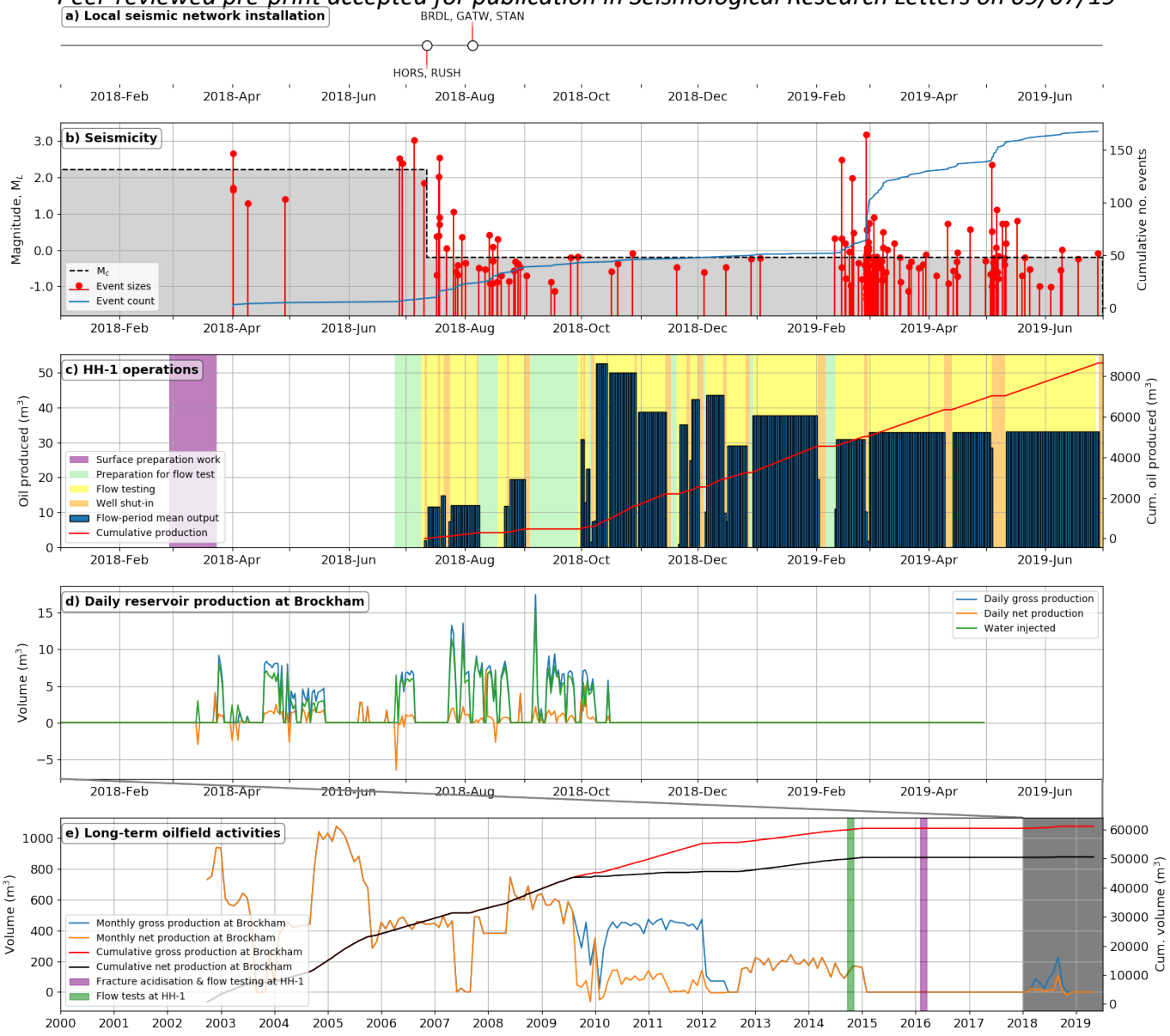

Figure 3: Timeline comparing evolution of the Newdigate seismic swarm with nearby oil field activities. a) Installation dates of the local temporary seismic monitoring network. (a) detected seismicity, cumulative number of events, and the grey shaded area indicating the approximate completeness magnitude of the catalogue over time. (c) Horse Hill-1: operations timeline (shaded boxes) together with flow-period averaged production and cumulative production over time. d) Daily reservoir production and injection values at Brockham. (e) A long-term view of operations, with the time interval shown in panels above covering the 2018–2019 period delineated by the grey box and connecting lines.

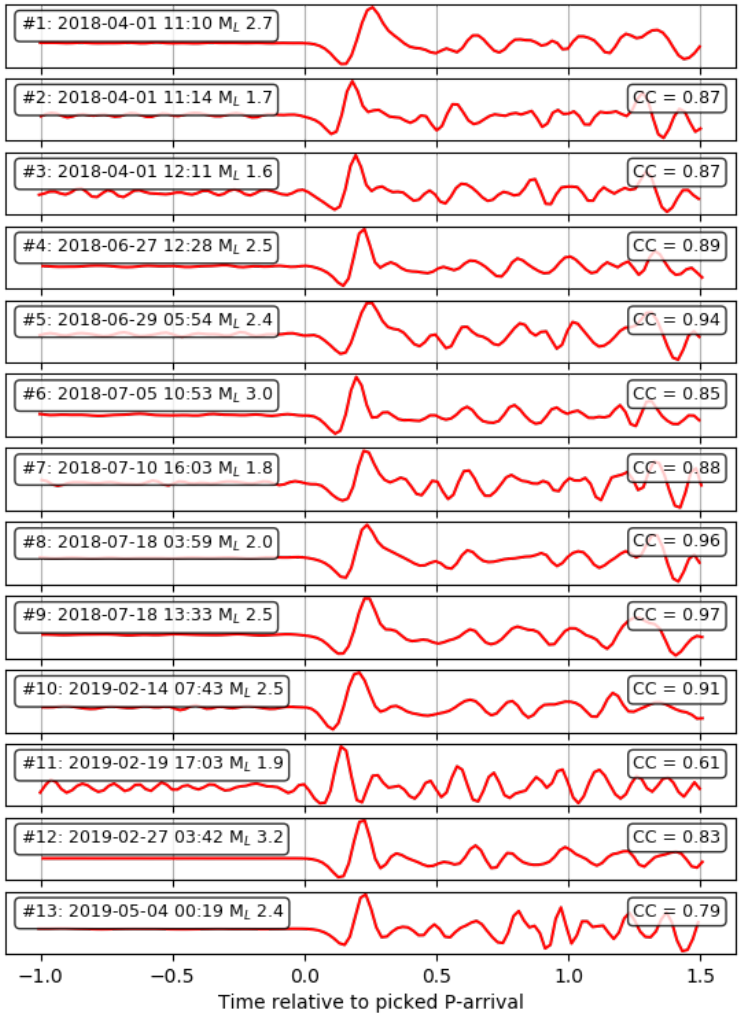

Figure 4: Lowpass-filtered (10 Hz) vertical-component waveforms recorded at RaspberryShake (RS) station REC60 (~8 km epicentral distance) showing similarity between the largest events (M_L > 1.5) of the Newdigate sequence. Waveform cross-correlation (CC) values computed in a window starting 0.02 s and ending 0.70 s after the picked P-wave arrival are labelled and are calculated with respect to the first event in the sequence (#1).

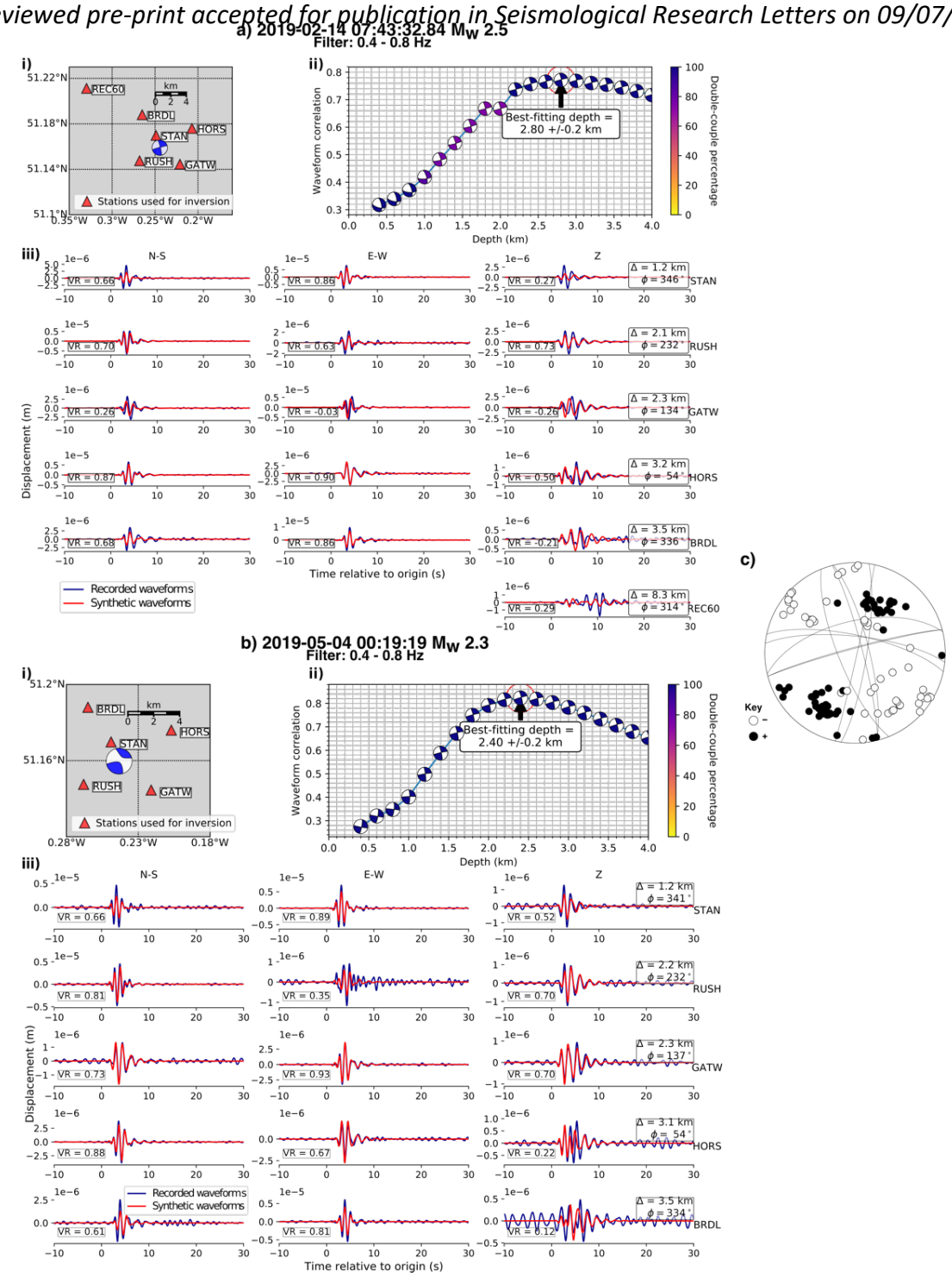

Figure 5: a) and b) Moment tensor solutions for two earthquakes observed by local stations. i) Map showing stations and best-fitting focal mechanism; ii) waveform correlation as a function of centroid depth; iii) waveform fits. "VR" = variance reduction. c) Observed first-motion P-wave polarities compared to faults planes from the best-fitting focal mechanisms from moment tensors a) and b).

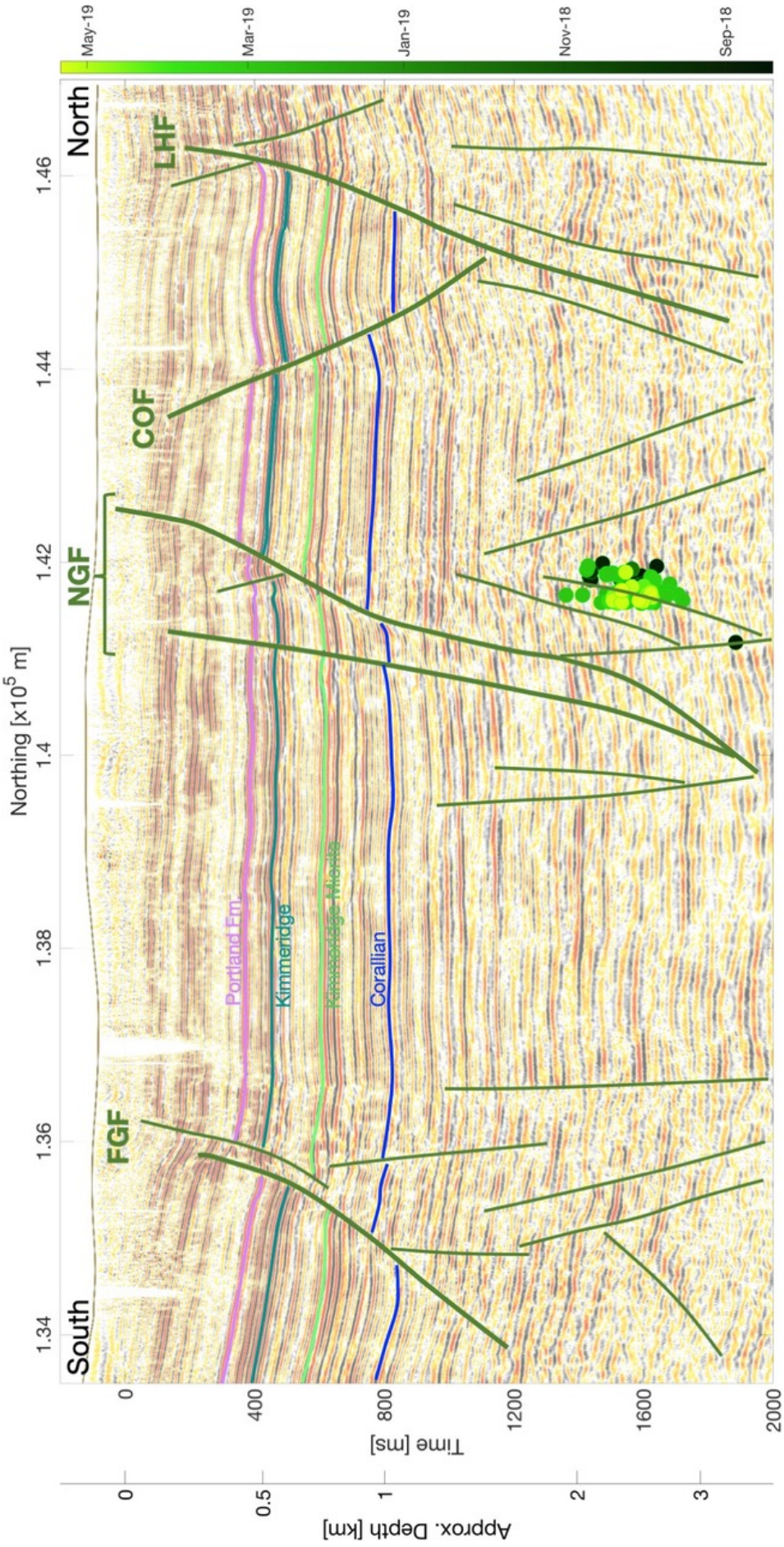

Figure 6: 2-D seismic section along profile TWLD-90-15 (Figure 2) showing interpreted faults (green lines), geological formations, together with the projected positions of relocated earthquakes from this study. Poorly constrained event with fixed depths are shown as squares; well-constrained events are shown as circles. Event location are also given as dashed error bars. COF = C = Collendean Fault; FGF = Faygate Fault; LHF = Leigh Fault; NGF = Newdigate Fault.

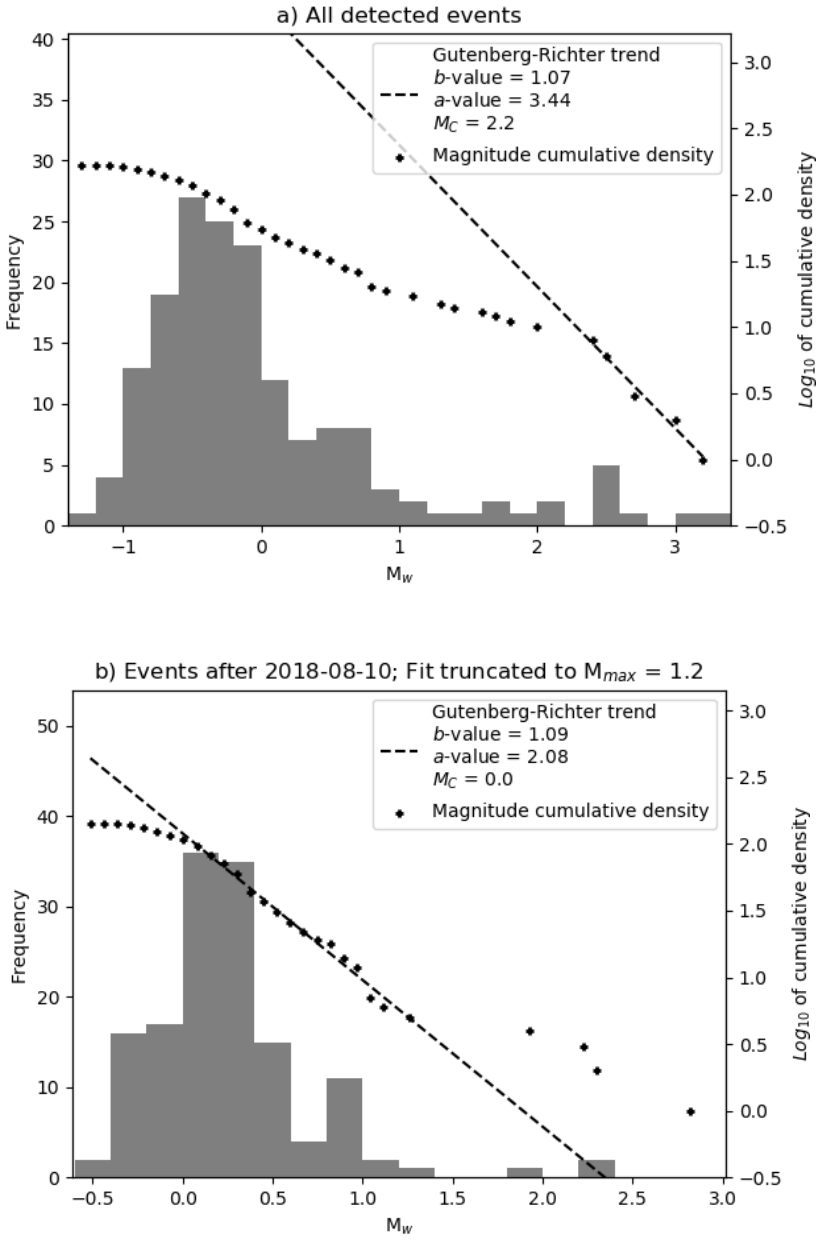

Figure 7: Individual and cumulative frequency-magnitude distributions together with Gutenberg-Richter (G-R) relationship fits for a) the entire sequence and b) the sequence recorded by the temporary local monitoring network, with magnitudes scaled to an equivalent M_w, and G-R fits truncated to maximum magnitude of 1.2.